Applied Ocean Research 116 (2021) 102868

Contents lists available at ScienceDirect

Applied Ocean Research

journal homepage: www.elsevier.com/locate/apor

Guaranteed cost control for dynamic positioning of marine surface vessels with input saturation

Tao Liu [a], Yunfei Xiao [a], Yuan Feng [a], Jun Li [a], Bing Huang [b,*]

[a] College of Automation, Harbin Engineering University, Harbin, 150001, China
[b] Science and Technology on Underwater Vehicle Laboratory, Harbin Engineering University, Harbin, 150001, China

ARTICLE INFO

Key words:
Marine surface vessels
Guaranteed cost control
Input saturation
Linear matrix inequalities

ABSTRACT

This paper investigates the dynamic positioning (DP) control problem of marine surface vessels (MSVs) suffering from external perturbations and input saturation. The linear Matrix Inequalities (LMI) based guaranteed cost control scheme is designed to obtain the satisfaction of the preset performance indicators. Aiming towards this purpose, the mathematical model of the MSV is first translated into a novel state-and-parameter-dependent (SPD) structure under small yaw angle variation. Furthermore, the performance indicator of the control scheme is derived for robustness against disturbances. With the application of LMI analysis method, the performance function will be transformed to a matrix inequality. Then, input saturation constraints are imposed to the control input, which will also be treated as a matrix inequality. Eventually, theoretical analysis shows that asymptotic stability will be endowed to the closed-loop system and input saturation constraints are also satisfied. Numerical simulation results are presented to demonstrate the advantage and validity of the proposed controller.

1. Introduction

In the past few decades, with the constantly depletion of terrestrial energy, the abundant energy resources under the sea bed are exciting an ever-increasing attentions of offshore resource exploitation (B Huang et al., 2021; B Huang et al., 2021; Zhu et al., 2021). With intriguing applications in ocean engineering, dynamic positioning system (DPS) has provided a promising solution to stabilize marine vehicles around intended positions. In effect, as a station-keeping technique, the DPS can maintain vehicles at a fixed position and orientation even when encountering various kinds of ocean disturbances. In order to prevent the vessels drifting away from the rectification point, various control strategies involving PID control to optimal control were introduced into the DPS (Hu et al., 2021; Zhang et al., 2020; Y Huang et al., 2021) to achieve a satisfactory position keeping accuracy. Furthermore, superior to the traditional anchored positioning system, DPS possess a better adaptability in deep-sea maneuverability. By virtue of these, DPS is deemed to be an excellent alternative in diverse marine industries, such as pipe-laying, surveying, drilling and the exploitation of offshore resources (H Qin et al., 2020; H Qin et al., 2020), to name just a few.

With the burgeoning development of nonlinear control technologies, substantial efforts have been made for the controller design of marine vehicles. Since accurate parameters of vehicles remain inaccessible on realistic occasions, controllers with the capability of nonlinear approximation are highly demanded in real implementations. To this end, constructing nonlinear controllers with the integration of fuzzy logic (Ma et al., 2020; Wang and He, 2019) and neural networks (Zhou et al., 2021; Liu et al., 2020; Liu et al., 2015) were widely investigated. Moreover, to optimize transient and steady-state performance around the equilibrium position, a nonlinear error mapping function was embedded into the DPS controllers to account for the increasingly stringent demands of tasks (Wang et al., 2021). However, the negative impact of external ocean disturbances is nonnegligible when the results of (Gao et al., 2019) applied into reality. On this account, a bias observer was technically proposed with extra wave filter to accommodate the slow time-varying environmental loads (Værnø et al., 2019). Though somehow effective, one notable caveat is that the ocean waves are not the only factor leading to the performance deterioration in practice, as stated in the preceding paragraph. To proceed further, by incorporating the optimum observer-based technique into backstepping design in (Jayasiri et al., 2017), a robust controller was introduced as an effective solution to real-time DPS of MSVs with disturbance resistance in ice-infested waters. Although the fact that the foregoing control schemes seem feasible, the input constraints are a remaining challenge.

* Corresponding author.
E-mail address: binhuang@mail.nwpu.edu.cn (B. Huang).

https://doi.org/10.1016/j.apor.2021.102868
Received 20 April 2021; Received in revised form 1 September 2021; Accepted 6 September 2021
Available online 16 September 2021

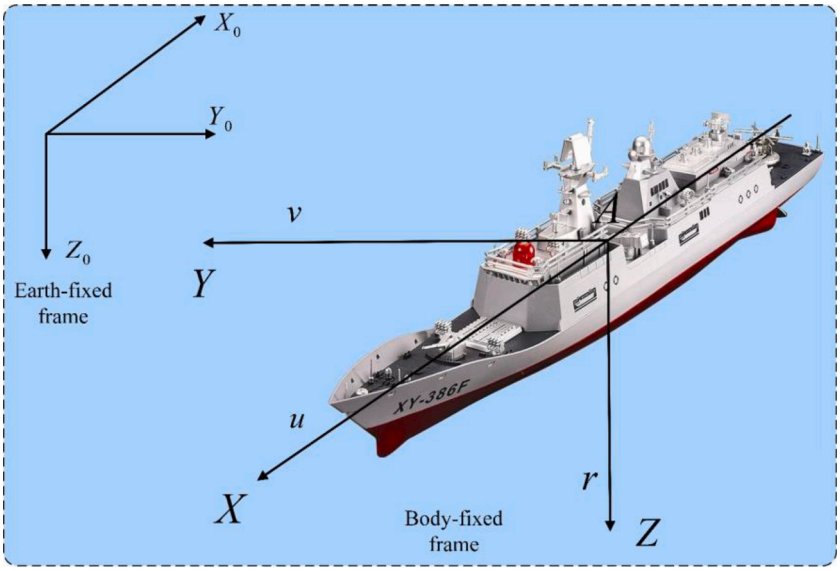

Fig. 1. Earth-fixed frame and body-fixed frame.

Except for nonlinear problem, another practically important issue that deserves attention in MSVs' applications is input saturation. Input saturation constraints always inevitably affect the performance of marine vehicles due to the limited power of propulsion system. Given the fact that the inherent physical restriction of the actuator always exists in practice, the input magnitude is therefore constrained and results in the degradation of the control performance, such as large overshoots or even the collapse of the system (Wang and Sun, 2021). Thereby, taking the input constraint into account has become an imperative in controller design, especially for the vessel and multiagent systems (Wang and Sun, 2018; Q Wang et al., 2019) that operating in harsh environments with large disturbing forces. To release this restriction, auxiliary systems were introduced into a backstepping technique in (Li et al., 2020; Du et al., 2016) for compensating the adverse effect enticed by input constraint. And then, the further step has been taken in (Liang et al., 2020), where the sliding mode control technique, which was to adopted for the avoidance of "explosion of complexity" inherent in backstepping. Totally different from the anti-windup algorithm with an auxiliary system in (Li et al., 2020; Du et al., 2016; Liang et al., 2020), a dead-zone based model of saturation phenomena was artfully established in (Shahriari-Kahkeshi, 2018) to replace the signum description, which qualifies for the job of achieving favorable performance metrics under the joint exploitation of robust and adaptive design.

To relax the conservativeness of the aforementioned results and guarantee a sufficient level of performance, the so-called guaranteed cost control is therefore devised in this brief with the linear quadratic cost function. Considering the unavoidable parameter perturbations induced by the deviations between digital models and real-world equipment, the optimal guaranteed cost control approach emerged in (Liu et al., 2014) to put an inferior limit for the performance deterioration, therefore somehow intensifying the control performance. More specially, since the vessel ought to move at a low speed when passing through narrow areas, the disturbance caused by wind is nonnegligible in (J Wang et al., 2019). On this account, Wang et al. (J Wang et al., 2019) investigated a robust H_∞ guaranteed cost controller to achieve a better path-following performance. Furthermore, aiming at removing the restriction of the transmission delays, a logarithmic quantizer is embedded into a guaranteed cost control algorithm to overcome the insufficiency of continuous-time communication (Lu et al., 2014). Similarly, the control bottleneck in time-delay systems, such as biological systems and metallurgical processing systems, has been broken by using a LMI approach incorporating with guaranteed cost control methods, as clearly stated in the work of (Xie and Lam, 2018). The preceding results have motivated our further research on the guaranteed cost control theory, i.e., extending its application to the DPS, as shown in this paper.

Motivated by the above discussion, a guaranteed cost controller based on LMI is proposed here to achieve DP of surface vessels in the case of input saturation constraint. The main contributions of the paper are summarized as follows:

(i) A guaranteed cost controller is put forward and sufficient conditions for asymptotic stability of the closed-loop system are given by using the LMI method. At the same time, the closed-loop system with disturbances can satisfy certain performance indexes. Different from the existing methods of anti-saturation (Værnø et al., 2019; Jayasiri et al., 2017; Wang and Sun, 2021), the input saturation problem is solved by transforming the system performance index and amplitude constraint of the system input into a series of solvable linear matrix inequalities.

(ii) Converting the kinematic and dynamic equations of surface vessel into a novel SPD structure is used for the controller and Lyapunov function, which can bring less conservativeness and more convenience than published literature (Hu et al., 2021; Zhang et al., 2020; Y Huang et al., 2021). Compared with the stabilization problem of DPS in (Fossen and Strand, 1999; Wu et al., 2018), the energy cost consumption for the surface vessels in DP can be significantly reduced by the presented guaranteed cost control which is conducive to practical applications.

The rest of this paper is structured as follows. In Section 2 system dynamics and preliminaries are provided, while Section 3 is dedicated to the main results. The simulation results are given in Section 4 to verify the effectiveness of the proposed control scheme. Finally, the conclusions are stated in Section 5.

2. System dynamics and preliminaries

In this paper, we consider that the desired trajectory of DPS is defined on the horizontal plane, where the earth-fixed frame and body-fixed frame are utilized to describe the planar motions of the surface vessel, which are shown in Fig. 1:

Referring to (Hu et al., 2020), the kinematic and dynamic equations of the surface vessel in the DP operation are given in follows:

$$\dot{\boldsymbol{\eta}} = \boldsymbol{J}(\psi)\boldsymbol{v} \tag{1}$$

$$\boldsymbol{M}_0\dot{\boldsymbol{v}} = -\boldsymbol{D}_0\boldsymbol{v} + \mathbf{h}(\boldsymbol{\tau}) + \boldsymbol{d}(t) \tag{2}$$

where $\boldsymbol{\eta} = [x, y, \psi]^{\mathrm{T}}$, comprising the position vector (x, y) and heading angle ψ in the earth-fixed coordinate frame (EFCF); $\mathbf{v} = [u, v, r]^{\mathrm{T}}$ is composed of the corresponding linear velocity (u, v) and angular velocity r in the body-fixed coordinate frame (BFCF). Herein, $\boldsymbol{J}(\psi)$ is the rotation matrix between the BFCF and the EFCF, which is defined as follows:

$$\boldsymbol{J}(\psi) = \begin{bmatrix} \cos(\psi) & -\sin(\psi) & 0 \\ \sin(\psi) & \cos(\psi) & 0 \\ 0 & 0 & 1 \end{bmatrix} \tag{3}$$

Additionally, $\boldsymbol{h}(\boldsymbol{\tau}) = [h_1, h_2, h_3]^{\mathrm{T}}, |h_i| \le h_{i\max}$ is the real control signals and $h_{i\max}$ being the maximum allowable value of h_i.

Due to the control input signals are provided by the propulsion system. Thus, the physical constraints must be taken into account, which will cause magnitude constraints of the control input. The relation of τ_i and h_i could be summarized as follows:

$$h_i = \begin{cases} \tau_i, if|\tau_i| \le h_{i\max} \\ h_{i\max}, |\tau_i| > h_{i\max} \end{cases} \tag{4}$$

where τ_i is the desired command control to be designed. It can be deduced that the output of the designed controller in this paper always satisfies $|h_i| \le h_{i\max}$.

The vector $\boldsymbol{d}(t) = [\boldsymbol{d}_1(t), \boldsymbol{d}_2(t), \boldsymbol{d}_3(t)]^{\mathrm{T}}$ represents the lumped disturbances that composed by waves and ocean currents. For the kinetic equations presented in Eq. (2), $\boldsymbol{M}_0 \in \boldsymbol{R}^{3\times3}$ is the nominal part of the inertia matrix, $\boldsymbol{D}_0 \in \boldsymbol{R}^{3\times3}$ represents nominal part of the damping matrix, which is mainly caused by the linear wave drift damping and laminar skin friction. The detailed expressions and information for $\boldsymbol{M}_0$ and $\boldsymbol{D}_0$ of the parameters are shown in (Hu et al., 2020).

Assumption 1. When the yaw angle ψ is set as 0°, the equation $\boldsymbol{J}(\psi) \cong \boldsymbol{I}_{3\times3}$ can be pursued.

Remark 1. (Fossen and Strand, 1999) Considering the MSVs in the DP operation, yaw angle variation is very small and $\boldsymbol{J}(\psi) \cong \boldsymbol{J}(\psi + \psi_w)$ can be obtained. Here, ψ_w is denoted as a wave-induced yaw disturbance in which the magnitude is usually less than 5° in extreme weather situations (sea state codes 5–10) and less than 1° during normal operation of the vessel (sea state codes 1–5). Therefore, the equation $\cos(\psi + \psi_w) \cong \cos(\psi) = 1$ and $\sin(\psi + \psi_w) \cong \sin(\psi) = 0$ hold under $\psi = 0°$, as well as $\boldsymbol{J}(\psi) \cong \boldsymbol{I}_{3\times3}$. Thus, Assumption 1 is justified. (The reasonableness and correctness of Assumption 1 was subsequently verified in numerical simulations).

Remark 2. In practice, guaranteed cost control has been used in a wide range of applications, such as the application of guaranteed cost control in (LI et al., 2009) which improved transient performance and robustness with the aid of a two-stage inverted pendulum system. Similarly, guaranteed cost control is also commonly used in aerospace applications (Gao et al., 2011). Therefore, from a practical point of view, since the marine environment is both complicated and unpredictable, it may be difficult to observe the random disturbance of the surrounding environment in real time. Consequently, it is necessary to design a guaranteed cost controller with strong disturbance cancelation capability in the ocean realm.

Control objective: This paper mainly focuses on designing a guaranteed cost controller that can drive the position (x, y) and heading ψ of surface vessels located in the desired position and heading $\boldsymbol{\eta}_d = [x_d, y_d, \psi_d]^{\mathrm{T}}$ under the impact of external disturbances and input saturation constraints.

3. Main results

In this section, the guaranteed cost controller is designed based on LMI under the situation of external disturbances and input saturation. Since the current system is somehow defective in that the certain dynamic performance indicators are seldom considered, the research of guaranteed cost control is deemed to be meaningful in the high-requirement ocean missions. The main structure of residual section is organized into two parts, one is problem formulation and the other is the guaranteed cost controller design with input saturation.

3.1. Problem formulation

Firstly, the vessel motion mathematical equations are converted into a novel SPD structure to facilitate the controller design by virtue of LMI:

$$\dot{\boldsymbol{x}}(t) = \boldsymbol{A}\boldsymbol{x}(t) + \boldsymbol{B}[\boldsymbol{\tau}(t) + \boldsymbol{d}(t)] \tag{5}$$

$$\boldsymbol{y}(t) = \boldsymbol{C}\boldsymbol{x}(t) \tag{6}$$

where $\boldsymbol{x}(t) = \begin{bmatrix} \boldsymbol{\eta}(t) \\ \boldsymbol{v}(t) \end{bmatrix}, \boldsymbol{A} = \begin{bmatrix} 0 & I_{3\times3} \\ 0 & -\boldsymbol{M}_0^{-1}\boldsymbol{D}_0 \end{bmatrix}, \boldsymbol{B} = \begin{bmatrix} 0 \\ \boldsymbol{M}_0^{-1} \end{bmatrix}$ and $\boldsymbol{C} = \begin{bmatrix} \boldsymbol{C}_1 \\ \boldsymbol{C}_2 \end{bmatrix}$.

The guaranteed cost controller is constructed as:

$$\boldsymbol{\tau}(t) = \boldsymbol{K}\boldsymbol{x}(t) \tag{7}$$

where state-feedback gain $\boldsymbol{K}$ is 3×6 dimensional matrix in $\boldsymbol{x}(t)$.

Remark 3. The guaranteed performance controller can not only endow the vessels with disturbance-rejection property and suppress the chattering phenomenon, but also render it possible for the system state converging to the equilibrium in an exponential manner with guaranteed tracking performance metrics while effectively improving the dynamic properties of DPS. Furthermore, the feedback control gain $\boldsymbol{K}$ will be selected by subsequent LMI analysis to achieve the optimal performance.

The control objective of this section is to design controller Eq. (7), so that the asymptotic stability of the closed-loop system can be achieved, as well as the performance indicators defined in Eq. (8).

$$\int_0^\infty \boldsymbol{y}^T(t)\boldsymbol{y}(t)dt \le \gamma^2 \int_0^\infty \boldsymbol{d}^T(t)\boldsymbol{d}(t)dt \tag{8}$$

where the constant $\gamma > 0$.

Definition 1. Chen et al., 2004) If there exists a controller $\boldsymbol{\tau}$ and a positive scalar J^*, such that the nonlinear systems Eqs. (5) and ((6) are stable and the performance indicator function Eq. (8) satisfies $J = \int_0^\infty \boldsymbol{y}^T(t)\boldsymbol{y}(t)dt - \gamma^2 \int_0^\infty \boldsymbol{d}^T(t)\boldsymbol{d}(t)dt \le J^*$, then J^* is said to be a guaranteed cost and $\boldsymbol{\tau}$ is a guaranteed cost controller for the system of the surface vessel Eqs. (1) and (2).

Remark 4. For a nonlinear system satisfying a given quadratic performance index, it is difficult to design the optimal controller. However, this issue could be transformed to design a controller that can make the closed-loop system stable and can satisfy a quadratic index with a lower bound, which is called cost or performance. So guaranteed performance control is also called guaranteed cost control.

3.2. Guaranteed cost controller design with input saturation

In this section, a LMI based guaranteed cost DP control scheme is proposed for surface vessels with the consideration of input saturation and transient performance guarantee. In the following design, the guaranteed cost and input saturation constraints will be transformed into two matrix inequalities. Then, the LMI theory will be applied to find a feasible matrix $\boldsymbol{K}$ for Eq. (7). To better illustrate the design process, the

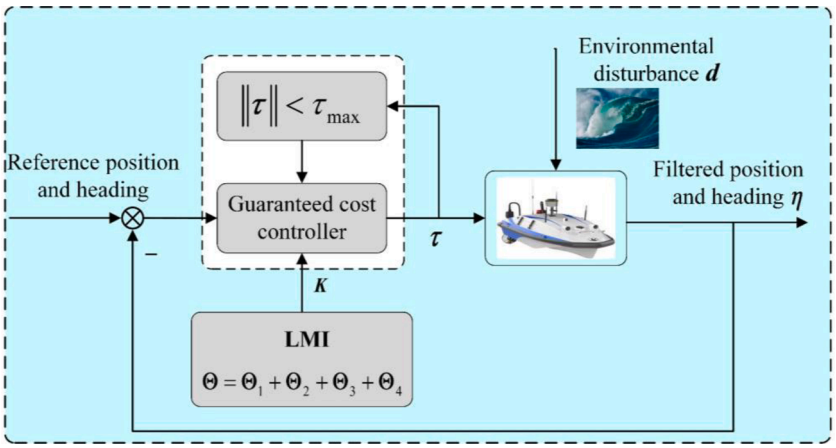

Fig. 2. The schematic diagram of the proposed method.

schematic diagram of the proposed method is depicted in Fig. 2.

Theorem 1. *For the nonlinear systems given in Eqs. (5) and (6) with the given parameter $\gamma > 0$, if there are positive definite symmetric matrixes $\boldsymbol{X} \in \boldsymbol{R}^{n\times n}$ and $\boldsymbol{Y} \in \boldsymbol{R}^{q\times n}$ satisfying the following matrix inequalities:*

$$\begin{bmatrix} \boldsymbol{AX} + \boldsymbol{XA}^T + \boldsymbol{BY} + \boldsymbol{Y}^T\boldsymbol{B}^T & \boldsymbol{B} & \boldsymbol{XC}^T \\ \boldsymbol{B}^T & -\gamma^2\boldsymbol{I} & 0 \\ \boldsymbol{CX} & 0 & -\boldsymbol{X} \end{bmatrix} < 0 \tag{9}$$

$$\boldsymbol{I} < \boldsymbol{X}^{-1} \tag{10}$$

$$\begin{bmatrix} \varpi^{-1}\tau_{\max}^2\boldsymbol{P} & \boldsymbol{K}^T \\ \boldsymbol{K} & \boldsymbol{I}_{3\times 3} \end{bmatrix} \geq 0 \tag{11}$$

where ϖ is a positive constant, $\boldsymbol{P} > 0, \boldsymbol{P} = \boldsymbol{P}^T$, $\tau_{maxi} = \max\{\tau_1, \tau_2, \tau_3\}$, the coefficient matrix $\boldsymbol{K}$ is defined as:

$$\boldsymbol{K} = \boldsymbol{YX}^{-1} \tag{12}$$

Then, the proposed controller Eq. (7) is able to endow the closed-loop system with asymptotical stability, as well as anti-saturation property and guaranteed performance.

Proof. Choose the following Lyapunov candidate:

$$V(\boldsymbol{x}(t)) = \boldsymbol{x}^T(t)\boldsymbol{P}\boldsymbol{x}(t) \tag{13}$$

Considering performance indicator Eq. (8), we defined:

$$J = \int_0^\infty \left[\boldsymbol{y}^T(t)\boldsymbol{y}(t) - \gamma^2\boldsymbol{d}^T(t)\boldsymbol{d}(t)\right]dt \tag{14}$$

To illustrate this performance indicator can be satisfied under the proposed controller, substituting Eq. (7) into Eq. (14), yields:

$$\begin{aligned} J &= \int_0^\infty \left[\boldsymbol{y}^T(t)\boldsymbol{y}(t) - \gamma^2\boldsymbol{d}^T(t)\boldsymbol{d}(t)\right]dt + V(\boldsymbol{x}(t)) - V(\boldsymbol{x}(t)) \\ &\leq \int_0^\infty \left[\boldsymbol{y}^T(t)\boldsymbol{y}(t) - \gamma^2\boldsymbol{d}^T(t)\boldsymbol{d}(t) + \dot{V}(\boldsymbol{x}(t))\right]dt \\ &= \int_0^\infty \{\boldsymbol{x}^T(t)\boldsymbol{C}^T\boldsymbol{C}\boldsymbol{x}(t) - \gamma^2\boldsymbol{d}^T(t)\boldsymbol{d}(t) \\ &\quad + [\boldsymbol{A}\boldsymbol{x}(t) + \boldsymbol{B}\boldsymbol{K}\boldsymbol{x}(t) + \boldsymbol{B}\boldsymbol{d}(t)]^T + \boldsymbol{P}\boldsymbol{x}(t) \\ &\quad \boldsymbol{x}^T(t)\boldsymbol{P}[\boldsymbol{A}\boldsymbol{x}(t) + \boldsymbol{B}\boldsymbol{K}\boldsymbol{x}(t) + \boldsymbol{B}\boldsymbol{d}(t)]dt\} \\ &= \int_0^\infty \{\boldsymbol{x}^T(t)\left[(\boldsymbol{A} + \boldsymbol{B}\boldsymbol{K})^T\boldsymbol{P} + \boldsymbol{P}(\boldsymbol{A} + \boldsymbol{B}\boldsymbol{K}) + \boldsymbol{C}^T\boldsymbol{C}\right]\boldsymbol{x}(t) \\ &\quad + 2\boldsymbol{x}^T(t)\boldsymbol{P}\boldsymbol{B}\boldsymbol{d}(t) - \gamma^2\boldsymbol{d}^T(t)\boldsymbol{d}(t)\}dt \end{aligned} \tag{15}$$

We can convert $\boldsymbol{I} < \boldsymbol{P}$ to $\boldsymbol{X} = \boldsymbol{P}^{-1}$ by using Eq. (10). Then, Eq. (15) can be further calculated as:

$$\begin{aligned} J &< \int_0^\infty \{\boldsymbol{x}^T(t)\left[(\boldsymbol{A} + \boldsymbol{B}\boldsymbol{K})^T\boldsymbol{P} + \boldsymbol{P}(\boldsymbol{A} + \boldsymbol{B}\boldsymbol{K}) + \boldsymbol{C}^T\boldsymbol{P}\boldsymbol{C}\right]\boldsymbol{x}(t) \\ &\quad + 2\boldsymbol{x}^T(t)\boldsymbol{P}\boldsymbol{B}\boldsymbol{d}(t) - \gamma^2\boldsymbol{d}^T(t)\boldsymbol{d}(t)\}dt \\ &= \int_0^\infty \left\{\begin{bmatrix}\boldsymbol{x}(t) \\ \boldsymbol{d}(t)\end{bmatrix}^T \begin{bmatrix}(\boldsymbol{A} + \boldsymbol{B}\boldsymbol{K})^T\boldsymbol{P} + \boldsymbol{P}(\boldsymbol{A} + \boldsymbol{B}\boldsymbol{K}) + \boldsymbol{C}^T\boldsymbol{P}\boldsymbol{C} & \boldsymbol{P}\boldsymbol{B} \\ \boldsymbol{B}^T\boldsymbol{P} & -\gamma^2\boldsymbol{I}\end{bmatrix}\begin{bmatrix}\boldsymbol{x}(t) \\ \boldsymbol{d}(t)\end{bmatrix}\right\}dt \end{aligned} \tag{16}$$

From (16), the $J < J^* = 0$ can be guaranteed only if the following inequality holds:

$$\Omega_0 = \begin{bmatrix}(\boldsymbol{A} + \boldsymbol{B}\boldsymbol{K})^T\boldsymbol{P} + \boldsymbol{P}(\boldsymbol{A} + \boldsymbol{B}\boldsymbol{K}) + \boldsymbol{C}^T\boldsymbol{P}\boldsymbol{C} & \boldsymbol{P}\boldsymbol{B} \\ \boldsymbol{B}^T\boldsymbol{P} & -\gamma^2\boldsymbol{I}\end{bmatrix} < 0 \tag{17}$$

Learning from Schur complement formula (Xie and Lam, 2018) and multiplying both sides of Ω_0 by $\mathrm{diag}(\boldsymbol{P}^{-1}, \boldsymbol{I})$ with the definitions $\boldsymbol{X} = \boldsymbol{P}^{-1}$ and $\boldsymbol{Y} = \boldsymbol{K}\boldsymbol{X}$. Thus, Eq. (9) of Theorem 1 is proven. Meanwhile, from the preceding analysis, one can deduce that our algorithm provides the possibility to achieve the preassigned performance with the form of Eq. (8).

Previous to demonstrate that the system possesses anti-saturation properties under the proposed controller, the asymptotic stability should be validated at first. For this purpose, we differentiating $V(\boldsymbol{x}(t))$:

$$\begin{aligned} \dot{V}(\boldsymbol{x}(t)) &= \dot{\boldsymbol{x}}^T(t)\boldsymbol{P}\boldsymbol{x}(t) + \boldsymbol{x}^T(t)\boldsymbol{P}\dot{\boldsymbol{x}}(t) \\ &= \boldsymbol{x}^T(t)\left[(\boldsymbol{A} + \boldsymbol{B}\boldsymbol{K})^T\boldsymbol{P} + \boldsymbol{P}(\boldsymbol{A} + \boldsymbol{B}\boldsymbol{K})\right]\boldsymbol{x}(t) + 2\boldsymbol{x}^T(t)\boldsymbol{P}\boldsymbol{B}\boldsymbol{d}(t) \\ &< \boldsymbol{x}^T(t)\left[(\boldsymbol{A} + \boldsymbol{B}\boldsymbol{K})^T\boldsymbol{P} + \boldsymbol{P}(\boldsymbol{A} + \boldsymbol{B}\boldsymbol{K})\right]\boldsymbol{x}(t) \\ &\quad + 2\boldsymbol{x}^T(t)\boldsymbol{P}\boldsymbol{B}\boldsymbol{d}(t) + \boldsymbol{d}^T(t)\boldsymbol{d}(t) \\ &= \begin{bmatrix}\boldsymbol{x}(t) \\ \boldsymbol{d}(t)\end{bmatrix}^T \begin{bmatrix}(\boldsymbol{A} + \boldsymbol{B}\boldsymbol{K})^T\boldsymbol{P} + \boldsymbol{P}(\boldsymbol{A} + \boldsymbol{B}\boldsymbol{K}) & \boldsymbol{P}\boldsymbol{B} \\ \boldsymbol{B}^T\boldsymbol{P} & \boldsymbol{I}\end{bmatrix}\begin{bmatrix}\boldsymbol{x}(t) \\ \boldsymbol{d}(t)\end{bmatrix} \end{aligned} \tag{18}$$

According to the Schur complement formula (Yu, 2002), one can deduced from the Eq. (17) that:

$$(\boldsymbol{A} + \boldsymbol{B}\boldsymbol{K})^T\boldsymbol{P} + \boldsymbol{P}(\boldsymbol{A} + \boldsymbol{B}\boldsymbol{K}) + \boldsymbol{C}^T\boldsymbol{P}\boldsymbol{C} + \gamma^2\boldsymbol{P}\boldsymbol{B}\boldsymbol{B}^T\boldsymbol{P} < 0 \tag{19}$$

It is indicated from (19) that the following inequality holds:

$$\begin{aligned} &(\boldsymbol{A} + \boldsymbol{B}\boldsymbol{K})^T\boldsymbol{P} + \boldsymbol{P}(\boldsymbol{A} + \boldsymbol{B}\boldsymbol{K}) - \boldsymbol{P}\boldsymbol{B}\boldsymbol{B}^T\boldsymbol{P} \\ &< (\boldsymbol{A} + \boldsymbol{B}\boldsymbol{K})^T\boldsymbol{P} + \boldsymbol{P}(\boldsymbol{A} + \boldsymbol{B}\boldsymbol{K}) + \boldsymbol{C}^T\boldsymbol{P}\boldsymbol{C} + \gamma^2\boldsymbol{P}\boldsymbol{B}\boldsymbol{B}^T\boldsymbol{P} \\ &< 0 \end{aligned} \tag{20}$$

Further conclusion is derived as:

$$\Omega_1 = \begin{bmatrix}(\boldsymbol{A} + \boldsymbol{B}\boldsymbol{K})^T\boldsymbol{P} + \boldsymbol{P}(\boldsymbol{A} + \boldsymbol{B}\boldsymbol{K}) & \boldsymbol{P}\boldsymbol{B} \\ \boldsymbol{B}^T\boldsymbol{P} & \boldsymbol{I}\end{bmatrix} < 0 \tag{21}$$

Since $\dot{V}(\boldsymbol{x}(t)) < 0$ is valid, $V(t) < V(0)$ holds certainly with $V(0) = \boldsymbol{x}^T(0)\boldsymbol{P}\boldsymbol{x}(0)$. On the basis of Eq. (21), the asymptotic stability of System Eqs. (5) and (6) is proven. If there exists a positive definite symmetric matrix $\boldsymbol{P}$ and a positive constant $\varpi > 0$, so that $\boldsymbol{x}^T(0)\boldsymbol{P}\boldsymbol{x}(0) < \varpi$ is true,

then $V(0) < \varpi$ can be guaranteed, and so it is $V(t) < \varpi$.

Regarding the input saturation problem in Theorem 1, according to Eq. (7), we can get:

$$\| \boldsymbol{\tau} \|^2 = [\boldsymbol{K}\boldsymbol{x}(t)]^T \boldsymbol{K}\boldsymbol{x}(t) = \boldsymbol{x}(t)^T \boldsymbol{K}^T \boldsymbol{K}\boldsymbol{x}(t) \tag{22}$$

Denoting $\boldsymbol{K}^T\boldsymbol{K} \leq \varpi^{-1}\tau_{maxi}^2\boldsymbol{P}$ and in the light of $V = \boldsymbol{x}(t)^T\boldsymbol{P}\boldsymbol{x}(t)$, it can be concluded that:

$$\| \boldsymbol{\tau} \|^2 \leq \varpi^{-1}\tau_{maxi}^2 V \leq \tau_{maxi}^2 \tag{23}$$

By Observing Eq. (23), it follows that:

$$\| \boldsymbol{\tau} \| \leq \tau_{maxi} \tag{24}$$

Based on the precondition shown in Eqs. (17) and (23), the efficacy of the inequalities Eqs. (9) and (11) can be further confirmed. Recalling the foregoing deduction, it is clear that the guaranteed performance can be obtained even in the consideration of saturation constraints.

Thus, completing the proof of Theorem 1.

Remark 6. Input saturation is regarded as one of the most common nonlinearities in nonlinear control systems. In practice, surface vessels always suffer from saturated control inputs, since the physical restriction of the actuator only gives limited access to the input signal. Given this fact, it is imperative to take precautions in an attempt to handle this constraint.

In the sequel, the control objective is to obtain the state feedback gain $\boldsymbol{K}$ through combing Eqs. (9)-(12). Schur complement formula is applied here to transform Eqs. (9)-(12) to four accessible inequalities.

Through the above analysis, it can be concluded that:

$$(\boldsymbol{A}+\boldsymbol{B}\boldsymbol{K})^T\boldsymbol{P} + \boldsymbol{P}(\boldsymbol{A}+\boldsymbol{B}\boldsymbol{K}) - \boldsymbol{P}\boldsymbol{B}(\boldsymbol{P}\boldsymbol{B})^T < 0 \tag{25}$$

$$\boldsymbol{K}^T\boldsymbol{K} - \varpi^{-1}\tau_{max}^2\boldsymbol{P} \leq 0 \tag{26}$$

Then, the constant $k_0 = \varpi^{-1}\tau_{max}^2$ is defined to solve the LMI. The transformation of Eq. (26) is taken as:

$$\begin{bmatrix} k_0\boldsymbol{P} & \boldsymbol{K}^T \\ \boldsymbol{K} & \boldsymbol{I}_{3\times3} \end{bmatrix} \geq 0 \tag{27}$$

Multiplying $\mathrm{diag}(\boldsymbol{P}^{-1}, \boldsymbol{I}, \boldsymbol{I}, \boldsymbol{I})$ in both sides of Eq. (27), it is obtained that:

$$\begin{bmatrix} k_0\boldsymbol{P}^{-1} & \boldsymbol{P}^{-1}\boldsymbol{K}^T \\ \boldsymbol{K}\boldsymbol{P}^{-1} & \boldsymbol{I}_{3\times3} \end{bmatrix} \geq 0 \tag{28}$$

By denoting $\boldsymbol{F} = \boldsymbol{K}\boldsymbol{P}^{-1}, \boldsymbol{N} = \boldsymbol{P}^{-1}$, it deduces that $\boldsymbol{P}^{-1}\boldsymbol{K}^T = \boldsymbol{F}^T$ holds. Considering Eqs. (25), (28) and the relation $\boldsymbol{P}^{-1}\boldsymbol{K}^T = \boldsymbol{F}^T$, the following LMI can be obtained:

$$\Theta_1 = \boldsymbol{N}\boldsymbol{A}^T + \boldsymbol{F}^T\boldsymbol{B}^T + \boldsymbol{A}\boldsymbol{N} + \boldsymbol{B}\boldsymbol{F} - \boldsymbol{B}\boldsymbol{B}^T < 0 \tag{29}$$

$$\Theta_2 = \begin{bmatrix} k_0\boldsymbol{N} & \boldsymbol{F}^T \\ \boldsymbol{F} & \boldsymbol{I}_{3\times3} \end{bmatrix} \geq 0 \tag{30}$$

On the basis of the definition of $\boldsymbol{P}$ and the fact of $\boldsymbol{P} > 0, \boldsymbol{P} = \boldsymbol{P}^T$, the following LMI can be deduced:

$$\Theta_3 = \boldsymbol{N} > 0 \tag{31}$$

In light of Schur complement formula, Eq. (31) exists due to the fact of $\boldsymbol{x}^T(0)\boldsymbol{P}\boldsymbol{x}(0) < \varpi$:

$$\Theta_4 = \begin{bmatrix} \varpi & \boldsymbol{x}^T(0) \\ \boldsymbol{x}(0) & \boldsymbol{N} \end{bmatrix} \geq 0 \tag{32}$$

The effective feedback control gain $\boldsymbol{K}$ can be confirmed from appropriately calculating the values of four LMIs $\Theta_1, \Theta_2, \Theta_3, \Theta_4$.

The guaranteed cost controller is put forward and the sufficient conditions for asymptotic stability of the closed-loop system are given by using the LMI method. At the same time, the closed-loop system with disturbances can satisfy certain performance indexes. Furthermore, system performance indexes and magnitude constraints of system inputs are properly transformed to a series of linear matrix inequalities. In this way, the control objective will be achieved just by seeking feasible conditions for these inequalities.

Table 1
The model parameters of MSV.

Description	Value	Unit
Mass	4.591×10^6	kg
Length	76.2	m
Inertia matrix $\boldsymbol{M}_0$	$\begin{bmatrix} 5.3122\times10^6 & 0 & 0 \\ 0 & 8.2831\times10^6 & 0 \\ 0 & 0 & 3.7454\times10^9 \end{bmatrix}$	− − −
Damping matrix $\boldsymbol{D}_0$	$\begin{bmatrix} 5.0242\times10^4 & 0 & 0 \\ 0 & 2.7229\times10^5 & -4.3933\times10^6 \\ 0 & -4.3933\times10^6 & 4.1894\times10^8 \end{bmatrix}$	− − −

Table 2
The initial values of MSV and the reference trajectory.

Description	Value
Initial position	$\boldsymbol{\eta}(0) = [20\ m, 20\ m, (10^\circ/180^\circ \times \pi\ rad)]^{\mathrm{T}}$
Reference point	$\boldsymbol{\eta}_d = [0\ m, 0\ m, 0\ rad]^{\mathrm{T}}$
Initial velocity	$\boldsymbol{v}(0) = [0\ m/s, 0\ m/s, 0\ rad/s]^{\mathrm{T}}$

Table 3
The parameters of the designed controller.

Parameter	Value
τ_{maxi}	$\max\{[1\times10^8\ N, 1\times10^8\ N, 1\times10^6\ N{\cdot}m]^T\}$
ϖ	50,000
γ	0.1
$\boldsymbol{P}$	$\begin{bmatrix} 0.2950 & 0.0057 & -0.0046 & 0.5766 & 0.0118 & 0.0211 \\ 0.0057 & 0.2903 & -0.0091 & 0.0069 & 0.7252 & 1.0834 \\ -0.0046 & -0.0091 & 0.4340 & -0.0057 & -0.0010 & 4.0234 \\ 0.5766 & 0.0069 & -0.0057 & 5.6143 & 0.0458 & 0.0486 \\ 0.0118 & 0.7252 & -0.0010 & 0.0458 & 7.4230 & 12.0682 \\ 0.0211 & 1.0834 & 4.0234 & 0.0486 & 12.0682 & 97.6549 \end{bmatrix}$
$\boldsymbol{K}$	$10^6 \times$ $\begin{bmatrix} -0.1543 & -0.0021 & 0.0030 & -0.8178 & -0.0053 & 0.0126 \\ -0.0022 & -0.1515 & 0.0044 & -0.0028 & -0.9760 & -1.9784 \\ -0.0002 & -0.0006 & -0.1389 & -0.0014 & -0.0132 & -1.1558 \end{bmatrix}$

4. Simulation

In this section, three numerical experiments are carried out to verify the effectiveness and the superiority of the anti-saturation guaranteed cost control approach. Firstly, the robustness of the proposed control algorithm is proved by comparative simulation experiments under three types of disturbances and system uncertainties. Then, two scenarios are adopted to illustrate that the proposed algorithm does effectively improve the control effect in the presence of input saturation constraints. Subsequently, the third experiment is conducted by comparing with the H_∞ optimal control strategy (Hu et al., 2020). Finally, by the above three experiments, we conclude that the proposed method will possess guaranteed cost with anti-saturation property.

The parameters of the supply vessel Northern Clipper (Fossen and Strand, 1999) are given in Table 1. In addition, the initial parameters of MSV are given in Table 2. The parameters of the designed controller are given in Table 3.

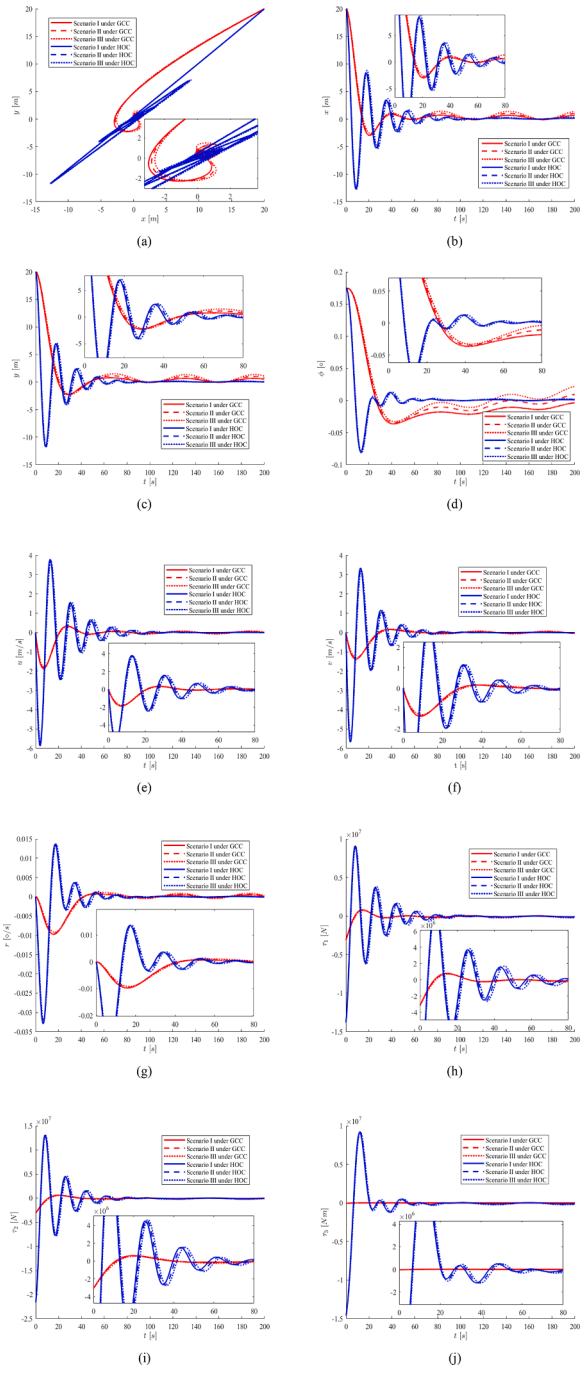

Fig. 3. Time responses of trajectories (a), positions x (b), y (c), yaw angle ψ (d), surge velocity (e), sway velocity v (f), yaw rate r (g), control forces τ_1 (h), τ_2 (i), and yaw moment τ_3 (j) under different disturbances and model uncertainties.

4.1. Comparison results under different disturbances and model uncertainties

Three schemes are used here and the robustness of the proposed controller (it is represented by GCC) is demonstrated by comparing it with H_∞ optimal control (it is represented by HOC) (Hu et al., 2020). For this purpose, we set three types of external disturbances and system uncertainties for simulations. The contrast simulated scenarios are specified as follows with the GCC consideration of input saturation given in Table 3. At the same time, in order to verify the rationality of Assumption 1, the heading angle ψ of the dynamic positioning vessel is defined as 8° instead of $\boldsymbol{J}(\psi) \cong \boldsymbol{I}_{3\times3}$, then the rotation matrix is shown as:

$$\boldsymbol{J}(\psi) = \begin{bmatrix} 0.99 & -0.139 & 0 \\ 0.139 & 0.99 & 0 \\ 0 & 0 & 1 \end{bmatrix}$$

Scenario I. Parameters $\boldsymbol{M}_0$ and $\boldsymbol{D}_0$ of the MSV have 0% uncertainties and the disturbances are given as:

$$\boldsymbol{d}(t) = 0.5 \times 10^5 \times \left[1 + \sin\frac{\pi}{30}t, 1 + cos\frac{\pi}{30}t, 1 + cos\frac{\pi}{30}t + \sin\frac{\pi}{30}t\right]^T$$

Scenario II. Parameters $\boldsymbol{M}_0$ and $\boldsymbol{D}_0$ of the MSV have 5% uncertainties and the disturbances are given as:

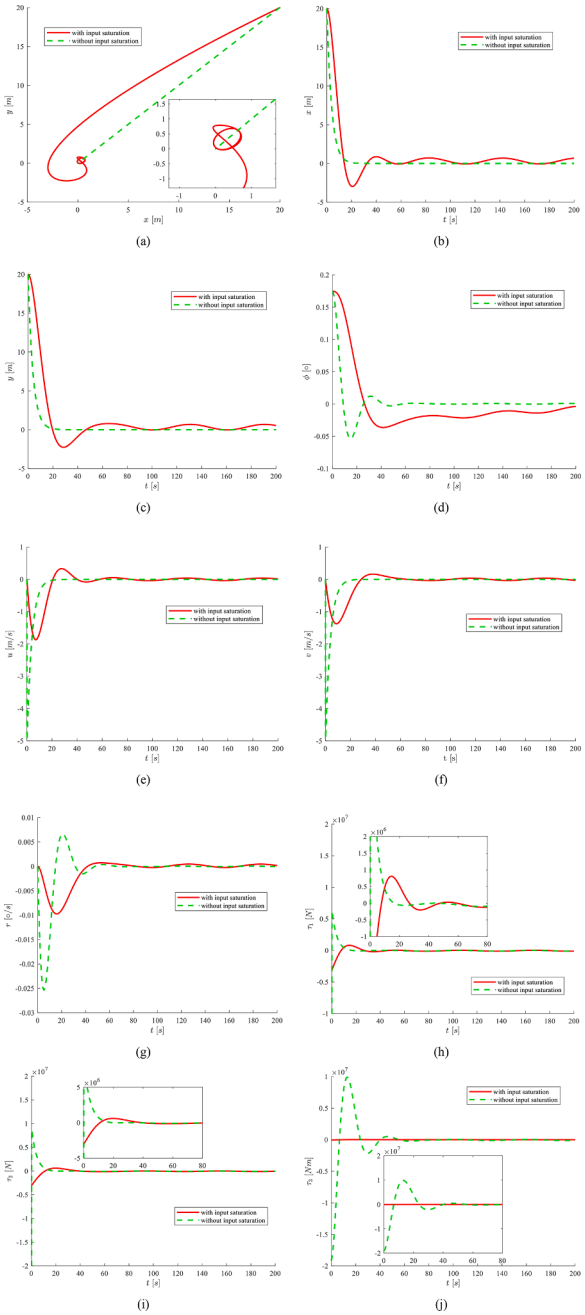

Fig. 4. Time responses of trajectories (a), positions x (b), y (c), yaw angle ψ (d), surge velocity (e), sway velocity v (f), yaw rate r (g), control forces τ_1 (h), τ_2 (i), and yaw moment τ_3 (j) with and without input saturation constraints.

$$\boldsymbol{d}(t) = 0.75 \times 10^5 \times \left[1 + \sin\frac{\pi}{30}t, 1 + cos\frac{\pi}{30}t, 1 + cos\frac{\pi}{30}t + \sin\frac{\pi}{30}t\right]^T$$

Scenario III. Parameters $\boldsymbol{M}_0$ and $\boldsymbol{D}_0$ of the MSV have 10% uncertainties and the disturbances are given as:

$$\boldsymbol{d}(t) = 1 \times 10^5 \times \left[1 + \sin\frac{\pi}{30}t, 1 + cos\frac{\pi}{30}t, 1 + cos\frac{\pi}{30}t + \sin\frac{\pi}{30}t\right]^T$$

The simulation results under Scenario I - III are depicted in Fig. 3(a) - (j). In Fig. 3, the time responses of DP trajectories are given in (a) and the time responses of positions x, y and yaw angle ψ are given in (b) - (d), respectively. As indicates in partial enlarged view of Fig. 3(a) - (d), the states of vessels were rapidly and smoothly regulated into a neighborhood of the reference point $\boldsymbol{\eta}_d = [0\ m, 0\ m, 0\ rad]^{\mathrm{T}}$ by the presented GCC algorithm. The time responses of velocities u, v and r are depicted in Fig. 3(e) - (g). From these results, it can be observed that velocity responses of the vessel were also quickly bounded into a small neighborhood of zero. In an overview of the results shown in Fig. 3(a) - (g), we can conclude that the control objectives of the vessel DP have been achieved in terms of response speed and control accuracy. Furthermore, by comparing the results of the two control methods under different scenarios, we can conclude that the obtained DP system is highly robust to external perturbations and model uncertainties. The time responses of control forces and moments $\tau_1(t), \tau_2(t), \tau_3(t)$ are drawn in Fig. 3(h) - (j), according to the enforced input saturation constraints in Table 3, we can observe that the saturation constraints of actuators were never violated. Meanwhile, it can be seen from partial enlarged view of Fig. 3(b) - (j) that the GCC algorithm has better vibration suppression performance to overcome the chattering phenomenon. Therefore, simulation proves that the proposed guaranteed performance controller can not only ensure the steady-state performance of the closed-loop system, but also improve the transient performance under different environmental conditions. In summary, these results prove the validity of Theorem 1 and the justifiability of Assumption 1.

4.2. Comparison result with and without the saturation constraint

Two scenarios are adopted here with and without the saturation constraint considered, respectively. Disturbances and uncertainties are the same as those in Scenario I, which is given in Section 4.1. In this subsection, the feedback control gain $\boldsymbol{K}$ is reset as:

$$\boldsymbol{K} = 10^8 \times \begin{bmatrix} -1.2235 & 0.3971 & 0.0036 & -3.3673 & 0.1184 & 0.0016 \\ 0.3318 & -1.2150 & 0.0031 & -0.0963 & -3.3902 & -0.0040 \\ 0.0019 & 0.0031 & -1.6710 & -0.0001 & 0.0003 & -2.5722 \end{bmatrix}$$

The simulation results of this subsection are given in Fig. 4. Among Fig. 4, the trajectory responses are given in (a) and the time responses of positions x, y and yaw angle ψ are given in (b) - (d), respectively. By observing these pictures, we can see that the control objective of DP can be achieved whether saturation constraint is considered and systems' performances are rarely affected by the input saturation constraints. To further illustrate the systems' responses under these two cases, the time responses of velocities and control forces are given in (e) - (g) and (h) - (j), respectively. Obviously, by comparing these results, when the input saturation is not considered, the control forces are much larger than the case when saturation is applied in the DP control scheme, which leaves the large energy consumption level of the platform. In summary, with the combination of all results depicted by Fig. 4, we can jump to the conclusion that under the proposed controller, the control objective of guaranteed cost can be achieved by the imposed input saturated constraints.

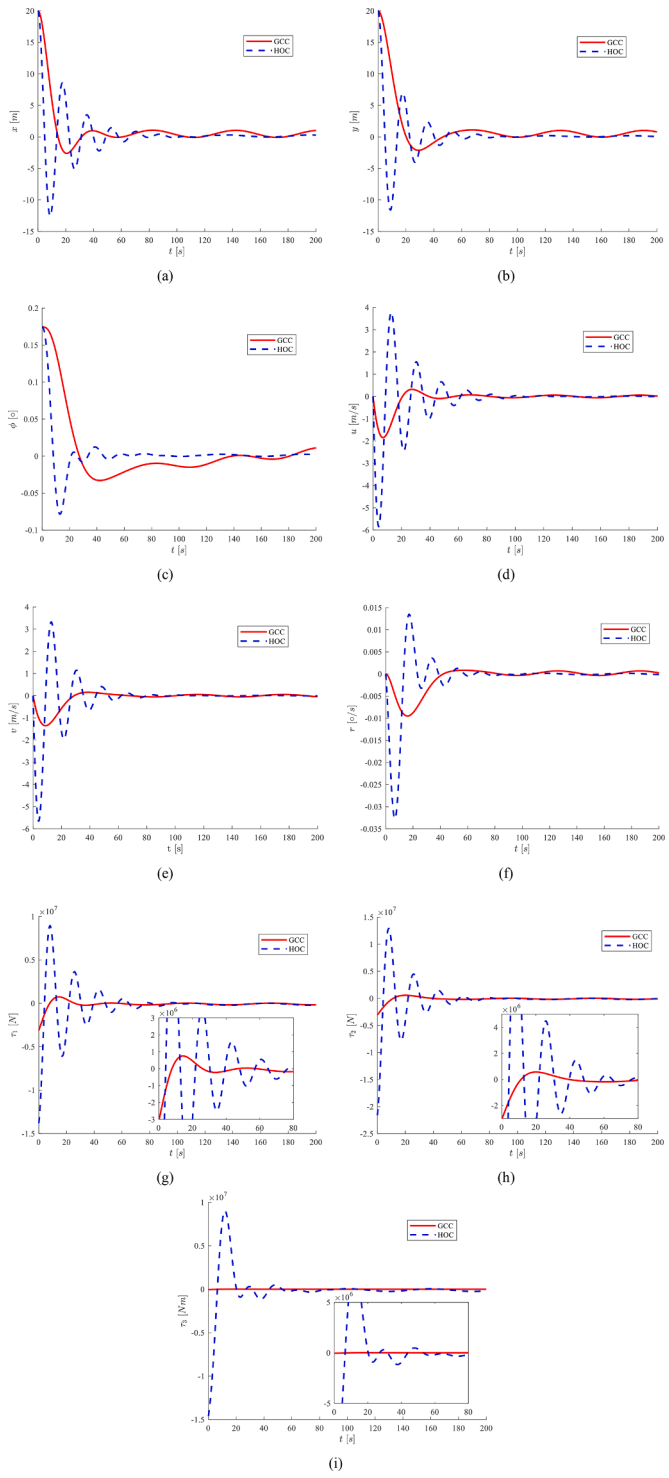

Fig. 5. Time responses of positions x (a), y (b), yaw angle ψ (c), surge velocity (d), sway velocity v (e), yaw rate r (f), control forces τ_1 (g), τ_2 (h), and yaw moment τ_3 (i) under different controllers.

4.3. Comparison result with H_∞ optimal control

In order to illustrate that the proposed guaranteed cost DP control scheme (denoted as GCC) can effectively reduce energy consumption, the H_∞ optimal control scheme (Hu et al., 2020) (denoted as HOC) is used here to be a comparative object. Additionally, the uncertainties and disturbances of the MSV are selected as scenario III in Section 4.1.

The simulation results of this subsection are given in Fig. 5. From

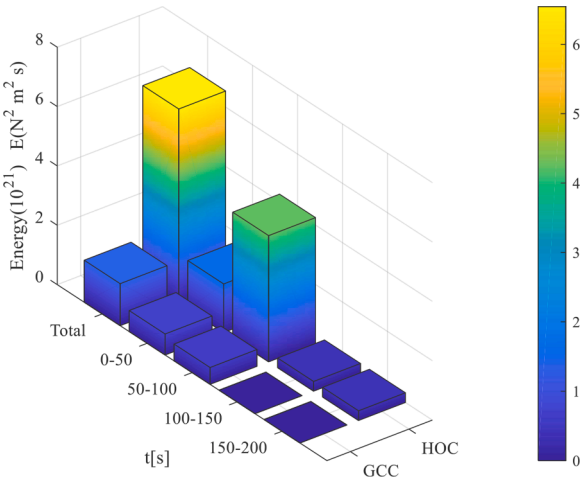

Fig. 6. Bar graphic visualization of energy consumption comparisons.

these results we can observe that the control goal of DP can be achieved by both algorithms. By comparing the time responses of x, y and ψ those given in (a) - (c), the presented GCC enjoys a much better controlled performance and anti-chatting ability than HOC since the trajectory responses of HOC are suffering from undesirable overshoots and oscillations. To further illustrate the control performance under these two DP control algorithms, the time responses of velocities are given in (d) - (f). Obviously, from (d) - (f) we can observe that the velocity responses under HOC are also suffering from the serve oscillations and have taken a long time to stable. To be specific, the set time of velocities under HOC are more than 80 s while the resulting DP system can be stabilized by the presented GCC before 40 s. To demonstrate the energy saving ability of the presented GCC, the time responses of control forces are given in (g) - (i). In viewing of these results, we can see that the responses of control forces under the presented GCC enjoys the advantages of lower control force requirements and fewer manipulation times than HOC. To evaluate the energy consumption level of these two algorithms, a performance index is adopted as follows.

$$E_{eng} = \int_0^t \boldsymbol{\tau}^T(\zeta)\boldsymbol{\tau}(\zeta)d\zeta \tag{33}$$

where t denotes the simulation time.

According to (33) and control force responses given in Fig. 5(g) - (i), the evaluation results of energy consumption levels are presented in Fig. 6. From Fig. 6, it can be observed that during the maneuvering period (i.e.: 0 s – 100 s), the presented GCC is much more energy saving since in this period, the total energy costing of HOC is 5.78×10^{21} N^2m^2s, while the only 1.07×10^{21} N^2m^2s of power is costed by the GCC. Therefore, comparing with the HOC method, the energy costing for the surface vessels in DP can be guaranteed by the presented GCC.

The foregoing comparative results verify that the DP control with guaranteed cost controller has strong robustness and adaptability to the environment disturbances. The comparative results show that the designed guaranteed performance control scheme has high computational efficiency and stable control performance, which is beneficial to practical applications, especially under the influence of disturbance forces in harsh environmental conditions and input saturation limit.

5. Conclusion

In this paper, a guaranteed cost controller for DP of surface vessels has been developed on the basis of LMI. Synthesized with anti-saturation design, the input saturation constraint is no longer an obstacle in DP issues. Moreover, owning the disturbance-rejection character endows the system with desirable adaptions to the harsh environment. Numerical simulation has validated the efficacy and superiority of our work.

In the future works, the simulation platform will not only stay on software view. The developed control scheme will be implemented on a small MSV designed by our laboratory to prove the effectiveness of the proposed control method in practice. Additionally, with the simultaneous consideration of input saturation, guaranteed cost and actuator faults for MSV control will be our future research direction.

CRediT authorship contribution statement

Tao Liu: Conceptualization, Methodology, Software, Validation, Formal analysis, Writing – original draft. **Yunfei Xiao:** Data curation, Investigation, Formal analysis, Writing – original draft. **Yuan Feng:** Validation, Writing – review & editing. **Jun Li:** Software, Validation, Writing – review & editing. **Bing Huang:** Supervision, Methodology, Formal analysis, Writing – original draft.

Declaration of Competing Interest

The authors declare that they have no conflict of interest concerning the publication of this manuscript.

Acknowledgments

This study was co-supported by the Fundamental Research Funds for the Central Universities (Nos. XK2010021018 and GK2010260338); Science and Technology on Underwater Vehicle Laboratory under Grant Nos. 6217905300000870562, 6142215190207 and JCKYS2020SXJQR-03; China Postdoctoral Science Foundation funded project (No. 2020M681081), and the project supported by Hei Long Jiang Postdoctoral Foundation (No. LBH-Z20130).

References

Huang, B., Song, S., Zhu, C., et al., 2021a. Finite-time distributed formation control for multiple unmanned surface vehicles with input saturation. Ocean Eng. 233, 109158.
Huang, B., Zhou, B., Zhang, S., et al., 2021b. Adaptive prescribed performance tracking control for underactuated autonomous underwater vehicles with input quantization. Ocean Eng. 221, 108549.
Zhu, C., Huang, B., Zhou, B., et al., 2021. Adaptive model-parameter-free fault-tolerant trajectory tracking control for autonomous underwater vehicles. ISA Trans 114, 57–71.
Hu, C., Wu, D., Liao, Y., et al., 2021. Sliding mode control unified with the uncertainty and disturbance estimator for dynamically positioned vessels subjected to uncertainties and unknown disturbances. Appl. Ocean Res. 109, 102564.
Zhang, G., Yao, M., Xu, J., et al., 2020. Robust neural event-triggered control for dynamic positioning ships with actuator faults. Ocean Eng. 207, 107292.
Huang, Y., Wu, D., Yin, Z., et al., 2021c. Design of UDE-based dynamic surface control for dynamic positioning of vessels with complex disturbances and input constraints. Ocean Eng. 220, 108487.
Qin, H., Li, C., Sun, Y., et al., 2020a. Adaptive trajectory tracking algorithm of unmanned surface vessel based on anti-windup compensator with full-state constraints. Ocean Eng. 200, 106906.
Qin, H., Li, C., Sun, Y., et al., 2020b. Finite-time trajectory tracking control of unmanned surface vessel with error constraints and input saturations. J. Franklin Inst. 357 (16), 11472–11495.
Ma, Y., Nie, Z., Yu, Y., et al., 2020. Event-triggered fuzzy control of networked nonlinear underactuated unmanned surface vehicle. Ocean Eng. 213, 107540.
Wang, N., He, H., 2019. Dynamics-level finite-time fuzzy monocular visual servo of an unmanned surface vehicle. IEEE Trans. Indust. Electron. 67 (11), 9648–9658.
Zhou, B., Huang, B., Su, Y., et al., 2021. Fixed-time neural network trajectory tracking control for underactuated surface vessels. Ocean Eng. 236, 109416.
Liu, L., Zhang, W., Wang, D., et al., 2020. Event-triggered extended state observers design for dynamic positioning vessels subject to unknown sea loads. Ocean Eng. 209, 107242.
Liu, L., Wang, D., Peng, Z, 2015. Direct and composite iterative neural control for cooperative dynamic positioning of marine surface vessels. Nonlinear Dyn 81 (3), 1315–1328.
Wang, Y., Wang, H., Li, M., et al., 2021. Adaptive fuzzy controller design for dynamic positioning ship integrating prescribed performance. Ocean Eng. 219, 107956.
Gao, X., Li, T., Shan, Q., et al., 2019. Online optimal control for dynamic positioning of vessels via time-based adaptive dynamic programming. J. Ambient Intell. Humaniz Comput. 1–13.

Værnø, S.A., Brodtkorb, A.H., Skjetne, R., 2019. Compensation of bias loads in dynamic positioning of marine surface vessels. Ocean Eng. 178, 484–492.
Jayasiri, A., Nandan, A., Imtiaz, S., et al., 2017. Dynamic positioning of vessels using a UKF-based observer and an NMPC-based controller. IEEE Trans. Autom. Sci. Eng. 14 (4), 1778–1785.
Wang, Q., Sun, C., 2021. A continuous distributed control algorithm for time-varying networks of nonlinear agents with input saturation. Int. J. Robust Nonlinear Control.
Wang, Q., Sun, C., 2018. Adaptive consensus of multiagent systems with unknown high-frequency gain signs under directed graphs. IEEE Trans. Syst. Man Cybernet.: Syst.
Wang, Q., Psillakis, H.E., Sun, C., 2019a. Cooperative control of multiple high-order agents with nonidentical unknown control directions under fixed and time-varying topologies. IEEE Trans. Syst. Man Cybernet.: Syst.
Li, J., Du, J., Hu, X., 2020. Robust adaptive prescribed performance control for dynamic positioning of ships under unknown disturbances and input constraints. Ocean Eng. 206, 107254.
Du, J., Hu, X., Krstić, M., et al., 2016. Robust dynamic positioning of ships with disturbances under input saturation. Automatica 73, 207–214.
Liang, K., Lin, X., Chen, Y., et al., 2020. Adaptive sliding mode output feedback control for dynamic positioning ships with input saturation. Ocean Eng. 206, 107245.
Shahriari-Kahkeshi, M., 2018. Dead-zone model-based adaptive fuzzy wavelet control for nonlinear systems including input saturation and dynamic uncertainties. Int. J. Fuzzy Syst. 20 (8), 2577–2592.
Liu, D., Wang, D., Wang, F.Y., et al., 2014. Neural-network-based online HJB solution for optimal robust guaranteed cost control of continuous-time uncertain nonlinear systems. IEEE Trans. Cybern. 44 (12), 2834–2847.
Wang, J., Zou, Z., Wang, T., 2019b. Path following of a surface ship sailing in restricted waters under wind effect using robust H∞ guaranteed cost control. Int. J. Naval Architect. Ocean Eng. 11 (1), 606–623.
Lu, R., Cheng, H., Bai, J., 2014. Fuzzy-model-based quantized guaranteed cost control of nonlinear networked systems. IEEE Trans. Fuzzy Syst. 23 (3), 567–575.
Xie, X., Lam, J., 2018. Guaranteed cost control of periodic piecewise linear time-delay systems. Automatica 94, 274–282.
Fossen, T.I., Strand, J.P., 1999. Passive nonlinear observer design for ships using Lyapunov methods: full-scale experiments with a supply vessel. Automatica 35 (1), 3–16.
Yu, L., 2002. Robust Control-LMI Approach. Publishing Company of Tsinghua, Beijing.
Hu, X., Wei, X., Zhang, H., et al., 2020. Composite anti-disturbance dynamic positioning of vessels with modelling uncertainties and disturbances. Appl. Ocean Res. 105, 102404.
Wu, D., Ren, F., Qiao, L., et al., 2018. Active disturbance rejection controller design for dynamically positioned vessels based on adaptive hybrid biogeography-based optimization and differential evolution. ISA Trans 78, 56–65.
Chen, W.H., Guan, Z.H., Lu, X., 2004. Delay-dependent output feedback guaranteed cost control for uncertain time-delay systems. Automatica 40 (7), 1263–1268.
LI, S., LU, R., WANG, J, 2009. Virtual reality simulation of inverted pendulum based on robust guaranteed cost control. Mech. Electric. Eng. Mag. 5.
Gao, X., Teo, K.L., Duan, G.R, 2011. Non-fragile guaranteed cost control for robust spacecraft orbit transfer with small thrust. IMA J. Math. Control Inf. 28 (4), 507–524.